N, S-Codoped TiO_2/Fe_2O_3 Heterostructure Assemblies for Electrochemical Degradation of Crystal Violet Dye

Pooja Sree, Palukuru; Vishnu Priya, Devangam A.; Dilip Kumar, Behara*[+]

Department of Chemical Engineering, JNTUA College of Engineering, Ananthapuramu, INDIA

ABSTRACT: *In contemporary research, "Heterostructure" assemblies play an important role in energy conversion systems, wherein the composite assemblies facilitate faster charge carrier transport across the material interfaces. The improved/enhanced efficiency metrics in these systems (electro/photo-electrochemical processes/devices) is due to synergistic interaction and synchronized charge transport across material interfaces. Herein, we report Type-I Heterostructure consists of N, S doped TiO_2 and Fe_2O_3 for electrochemical crystal violet dye degradation studies. Synthesized N-S codoped TiO_2/Fe_2O_3 composite heterostructured assemblies were fabricated on Titanium (Ti) substrate and used for electrochemical analysis. Complete decolorization was achieved with all the fabricated electrodes and a higher rate of degradation was achieved with the composite electrode ($Ti/TiO_2/Fe_2O_3$) in comparison to individual electrodes (bare Ti, Ti/TiO_2, Ti/Fe_2O_3). Further, a probabilistic mechanism of degradation is proposed in support of the hypothesis. The outcomes of present work will have a profound effect on doped semiconductor heterostructure assemblies in the degradation of complex dye molecules of industrial outlets.*

KEYWORDS: *Type-I Heterostructure, TiO_2, Fe_2O_3, Crystal violet dye.*

INTRODUCTION

Electrochemical oxidation process emerged as an important technique for the degradation of toxic or biorefractory organic pollutants from waste water [1-2]. As electrons are the sole agents involved in the organic pollutant abatement, these methods are eco- friendly, environmentally compatible and mostly preferred [3-4]. Further, they possess specific advantages over traditional methods such as the elimination of by-products formation, no additional requirement of chemicals, easy operation, high efficiency, cost-effective and provides safety as it operates under mild conditions [5]. An electrochemical process can be either direct or indirect oxidation processes. In direct oxidation, direct transfer of electron takes place at the anode and thereby degrade the pollutant adsorbed on the anode surface. In indirect oxidation, generation of hydroxyl radicals ($^{\bullet}OH$) takes place at the anode. The generated $^{\bullet}OH$ radicals act as strong oxidizing agents and readily react with organic pollutants, thereby oxidizing the pollutants to small molecules such as CO_2 and H_2O [3-8]. The electrode reaction at the anode is

$$M + H_2O \rightarrow M\,(^{\bullet}OH) + H^+ + e^- \quad (1)$$

Where M represents anode. The electrochemical generation of $^{\bullet}OH$ radicals and their chemical reactivity depends on the nature of the anode material used [9].

***** *To whom correspondence should be addressed.*

+ E-mail: dileepbh.chemengg@jntua.ac.in

1021-9986/2020/2/171-179 9/$/5.09

Therefore, electro-catalytic materials which are used as anode plays a significant role in electrochemical oxidation processes [10]. Hence, the selection and design of anode/catalytic material are crucial and specific characteristics such as high stability, electrochemical/ catalytic activity, over potential demands etc., has to be considered for effective degradation of organic pollutants [11-12].

In the recent past, semiconductors were used as noble anode materials in various catalytic/electro-catalytic/photo-catalytic/photo-electrochemical applications such as dye degradation, water splitting, CO_2 separation, and hydrogen storage [13-16]. It is mainly due to their extensive physical, chemical and readily tunable/modifiable properties either by size reduction or doping or sensitization to acquire desired properties of interest [17]. Semiconductors such as TiO_2 and Fe_2O_3 have attracted a great deal of attention for degradation of organic pollutants in comparison to other semiconductor materials owing to their hydrophilicity, abundant availability, stability, environmental compatibility, low cost and corrosion resistance [18-20]. However, the application of TiO_2 is limited due to its high band gap. Therefore, efforts have been made to decrease the optical band gap as well as to improve the electronic conductivity [21]. One way to achieve this is by doping with nonmetals such as nitrogen (N) and sulphur (S) which are *iso*-electronic with TiO_2. The added dopants will occupy the interstitial sites/oxygen vacancy sites of TiO_2 and lead to the formation of localized states just above the valence band [21-22]. Further, the formation of Type-I Heterostructure with a Fe_2O_3 material (having suitable band edge alignments with TiO_2) will facilitate charge carrier flow across material interfaces and improve the electrochemical activity [23]. Therefore, the Heterostructure assembly will promote charge carrier separation and increase the charge carrier lifetime owing to high adsorption capacity, and effective surface area [24].

Herein, we propose electrochemical degradation of crystal violet dye using N-S co-doped TiO_2/Fe_2O_3 composite heterostructured assemblies fabricated on titania (Ti) substrate. Titania substrate is chosen as good support due to its stability, and better conductivity [25-26]. It is hypothesized that the formed heterojunction will facilitate the faster charge carrier movements due to proper band edge alignments (CB edge of TiO_2 is -4.21 eV and CB edge value of Fe_2O_3 is -4.78 eV w.r.t Absolute Vacuum Scale [27]) and hence there is a net movement of charge carriers from TiO_2 to Fe_2O_3, which breaks the dye molecule at a faster rate. The fabricated electrodes were characterized using X-Ray Diffraction (XRD), Scanning Electron Microscopy (SEM), Energy Dispersive X-ray (EDX) spectroscopy, and Fourier Transfer InfraRed (FT-IR) spectroscopy. Further, to monitor electrochemical activity, analytical techniques such as cyclic voltammetry and UV-Vis spectroscopy measurements are used. The faster rate of decolorization is achieved with N, S-TiO_2/Fe_2O_3 electrode (~9h) in comparison to individual electrodes. This signifies the importance of iso-electronic non- metal (N, S) doped metal oxide Heterostructure in facilitating the fast charge carrier movements and thereby enhancing the electrochemical performance. The outcomes of the current article help not only in understanding the mechanism of dye degradation of complex molecules but also help to design low-cost catalytic Heterostructure assemblies for different catalytic/electro-catalytic applications.

EXPERIMENTAL SECTION

Materials and methods

Titanium isopropoxide [$Ti\{OCH(CH_3)_2\}_4$], Iron(III) nitrate nonahydrate ($Fe(NO_3)_3.9H_2O$), Ethanol (C_2H_5OH), Ammonia(NH_3), Thio-urea ($(NH_2)_2CS$), Sodium sulphate (Na_2SO_4), and Isopropyl alcohol (C_3H_8O) were purchased from Sigma Aldrich Chemicals (India) Ltd. Nafion(10%) liquid solution was purchased from Dupont Chemicals, USA. Crystal violet dye purchased from Sigma-Aldrich is used as a model pollutant in the present study. All the reagents were analytically grade and used as received without further purification. All solutions were prepared with distilled water.

Synthesis of un-doped and doped TiO_2 nanoparticles

9 mL of TTIP (Titanium tetra isopropoxide) is added dropwise to the homogeneous mixture of 150 mL of ethanol and 3.72 mL of distilled water after stirring for half an hour. The resultant mixture is stirred for 4 h at 85˚C under continuous magnetic stirring followed by centrifuge, dried at 60˚C in a hot air oven for 30 min and calcined at 400˚C for 3 h. Thus, Anatase TiO_2 nanoparticles are obtained. By adding the ammonia [5 mL], thiourea [9.3 g] as a precursor to the

above procedure N-TiO_2, S-TiO_2 nanoparticles are obtained respectively and adding both (2.5 mL, 5.4 g) N, S-TiO_2 nanoparticles are obtained [28]. The continuous magnetic stirring process was carried out in a fume hood.

Synthesis of Fe_2O_3 nanoparticles and N, S TiO_2/Fe_2O_3 nanocomposite

4 g of Fe $(NO_3)_3$. $9H_2O$ was dissolved in 100 mL of distilled water and was stirred for 30 min. 1.5 g of gelatin was added to 100 mL of distilled water and stirred for 30 min at 60˚C. Then the gelatin solution was slowly added to the iron nitrate solution and stirred for 1 h. Then the obtained gel is dried in hot air oven at 60˚C for 6 h and calcined at 600˚C for 1 h [29]. Thus Fe_2O_3 nanoparticles are formed. Adding 10 mg of prepared N, S-TiO_2 nanoparticles to the iron nitrate solution and following the above procedure then the N, S-TiO_2/Fe_2O_3 nanocomposite is obtained. Synthesis procedure of N, S-TiO_2/Fe_2O_3 nano-composites is shown in Fig.1.

Electrode fabrication

40 mg of nanoparticles/composite particles (i.e. TiO_2, Fe_2O_3, N, S-TiO_2/Fe_2O_3) was mixed with 2 mL of isopropanol and 20 µL of Nafion solution. Then, it was sonicated for 1 h and the slurry was applied onto the Ti plate (effective electrode surface area~ $1cm^2$), and dried at 60˚C on hot plate.

RESULTS AND DISCUSSION

Characterization of nanoparticles

XRD analysis

To study the crystalline nature of samples, XRD spectra of synthesized samples were taken from X-ray diffractometer with Cu K_α radiation (λ = 1.5406 A˚). Fig. 2 represents XRD spectra of TiO_2, N-TiO_2, S-TiO_2, N, S-TiO_2, Fe_2O_3 and N, S-TiO_2/Fe_2O_3 nanoparticles. The intense peaks at 2θ values of TiO_2, N-TiO_2, S-TiO_2, N,S-TiO_2 were observed at 25.48˚, 37.8˚, 47.8˚, 53.8˚, 62.6˚ which corresponds to (101), (004), (200), (105), (024) atomic planes respectively confirms the formation of tetragonal Anatase phase matching with JCPDS 21-1272 (Fig. 2(a)-2(d)) [21, 30-31]. The average crystallite size estimated for TiO_2, N-TiO_2, S-TiO_2, N, S-TiO_2 will vary in between 4-7 nm from Debye-Scherrer formula. The diffraction peaks of N-TiO_2 and S-TiO_2 samples were not shifted in comparison to TiO_2 sample indicating there is no crystal distortion upon doping. Also, the increase in intensity and narrowing the width of the diffraction peak of Anatase phase was observed for doped TiO_2 (Fig. 2(b)-2(d)) compared to pure TiO_2 (Fig. 2(a)). The results show that the doping of N and S into TiO_2 will increase the crystallite size and crystalline nature of the sample significantly.

Similarly, Fe_2O_3 exhibits peaks at 2θ values of 24.44˚, 30.2˚, 35.76˚, 43.4˚, and 62.91˚ corresponds to (012), (104), (110), (202), (214) indices confirms α- phase of Fe_2O_3 with JCPDS 03-0800 from Fig. 2(e) [32]. The average crystallite size of Fe_2O_3 nanoparticles was estimated to be 13 nm. Further, the diffraction peaks of N, S-TiO_2/Fe_2O_3 composite confirms the presence of both TiO_2 and Fe_2O_3 peaks as evident from Fig. 2(f). Moreover, the intensity of Anatase and α- phase peaks of N, S-TiO_2/Fe_2O_3 are attenuated signifying that they hinder the crystal growth of TiO_2 or Fe_2O_3 particles. Overall diffraction patterns from XRD spectra indicate the highly crystalline nature of Anatase phase TiO_2, α-Fe_2O_3 and N, S-TiO_2/Fe_2O_3 samples.

SEM and TEM analysis

The surface morphology of nanoparticles can be determined using Field Emission Scanning Electron Microscopy (FESEM), and elemental composition can be obtained by Energy Dispersive X-ray Spectroscopy (EDS). The surface material distribution of TiO_2 and N-S TiO_2 is shown in Fig. 3. However, the distribution is not uniform after doping in case of N, S-TiO_2. It may be probably due to surface segregation of the added dopants, and the lattice was completely distorted which was confirmed from SEM images Fig. 3. The spherical shape of TiO_2 was observed from Fig. 3(a). Inset Fig. 3(a) represents the EDS spectra which confirms the presence of Ti and O in the synthesized nanoparticles (Ti - 50.68%, O - 49.32%). The irregular shape of N, S-TiO_2 was observed from Fig. 3(b) which may be due to slight destruction in crystal lattice upon doping. Further, the surface texture and rough morphology shown in co-doped sample in comparison to pristine TiO_2 confirm the change in an electrochemical surface area available for catalytic activity. Further, to confirm the heterostructure formation, TEM analysis is performed (Fig. 3c). It can be clearly observed that the nanostructures are composed of N-S, co-doped TiO_2 and Fe_2O_3 which are widely distributed on entire surface as heterostructure

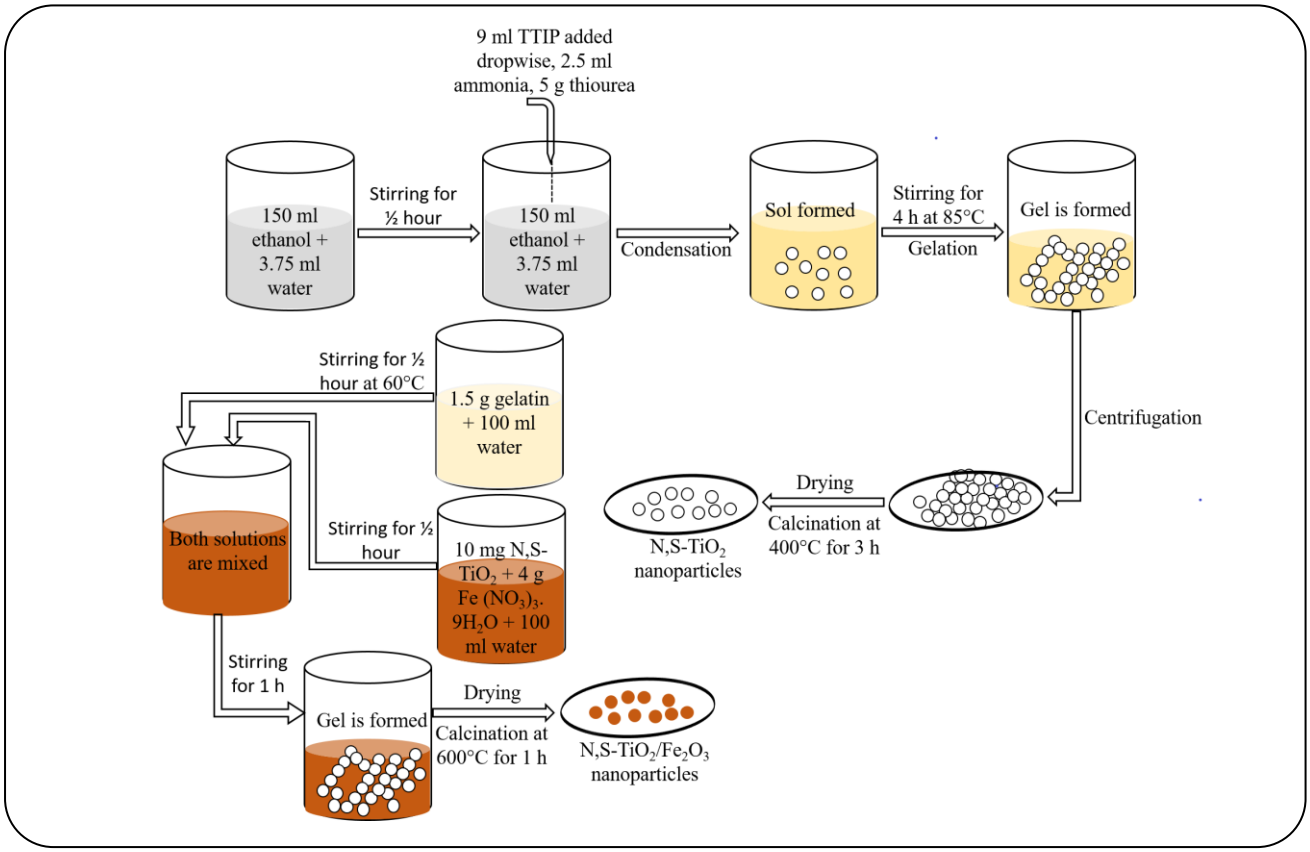

Fig. 1: Experimental procedure for the synthesis of N, S-TiO_2/Fe_2O_3 nanoparticles.

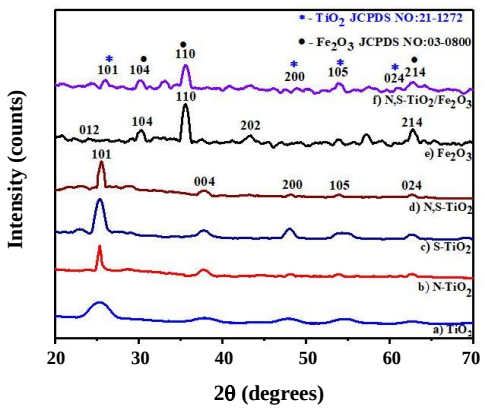

Fig. 2: XRD pattern of (a) TiO_2, (b) N-TiO_2 (c) S-TiO_2 (d) N, S-TiO_2 e) Fe_2O_3 f) N,S-TiO_2-Fe_2O_3 nanoparticles.

assembly/composite matrix (Fig. 3c, 3d). The d-spacing observed to be 0.24 nm corresponds to (103) plane of TiO_2 and 0.37 nm corresponds to (012) plane of α- Fe_2O_3 (Fig. 3d) which confirms the presence of two materials in heterostructure formation (the inset image shows zoomed portion of lattice fringes of Fe_2O_3).

FT-IR analysis

The FT-IR spectrum gives the information about the surface functional groups present on the surface of nanoparticles. The broadband observed at 3483 cm^{-1} represents the presence of hydroxyl groups on the surface of the sample which is significant factor in affecting electrochemical activity. The more the number of hydroxyl groups the faster the electro-catalytic degradation. The band at 2020 cm^{-1} signifies the deformation vibration of OH groups linked with titanium atoms (Ti-OH), and the band at 665cm^{-1} corresponds to titania crystal lattice vibrations from Fig. 4(a)-4(d). The band at 3418cm^{-1} and 1854 cm^{-1} were assigned to N-H stretching and bending vibrations of ammonium species from Fig. 4(b). No peak at 3483 cm^{-1} (OH) indicates that nitrogen is present only in the form of ammonium group on the surface. The band at 2782 cm^{-1} implies the -NCS stretching vibrations indicates the presence of nitrogen and Sulphur linkages on the surface of N, S-TiO_2 sample, and the surface adsorbed SO_4^{2-} species has a band at 1256 cm^{-1} corresponds to the asymmetric stretching vibrations of S=O from Fig. 4(c),4(d) [33-34]. The peak at 583.54 cm^{-1}

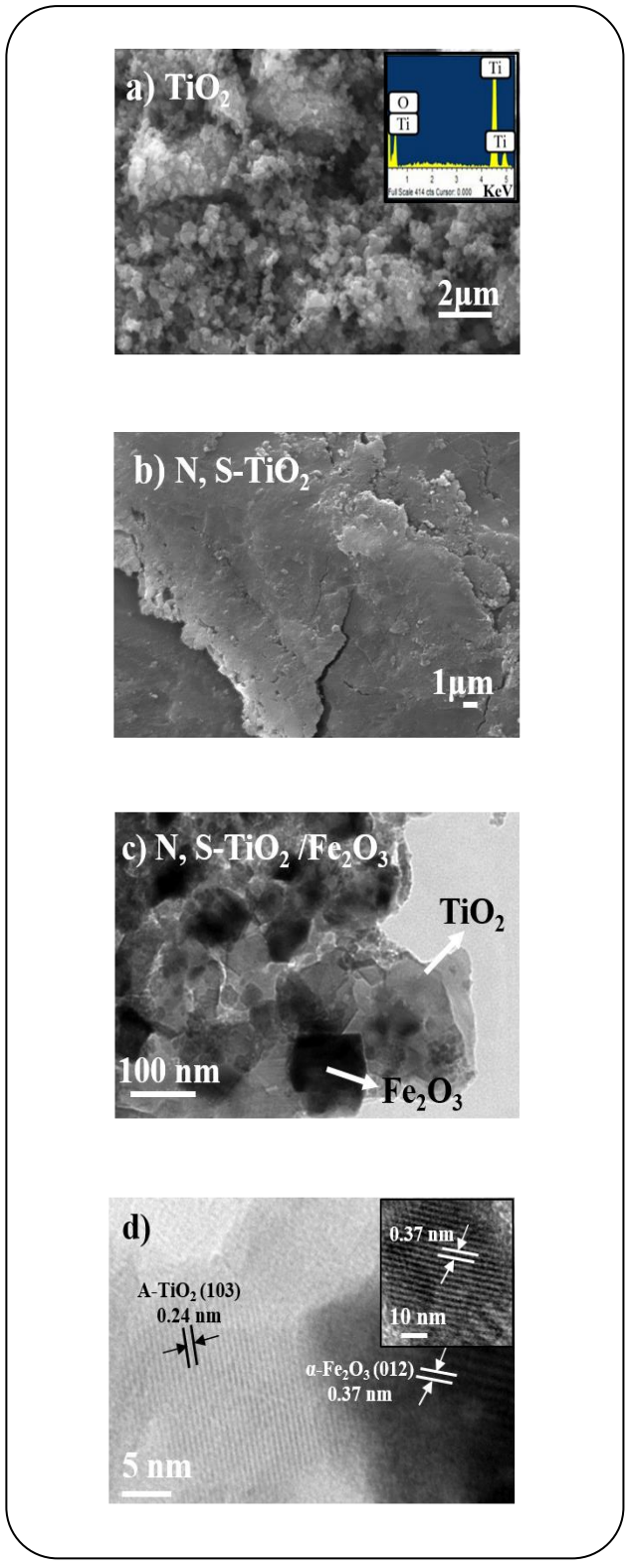

Fig. 3: FE-SEM images of (a) TiO_2 (b) N, S- TiO_2 nanoparticles (inset image shows EDS pattern); c) TEM, and d) HRTEM images of N, S-TiO_2/Fe_2O_3 nanoparticles (inset image shows lattice spacing).

represents to Fe-O stretching mode, the band at 3452 cm^{-1} were assigned to O-H stretching vibrations of surface water molecules and the band at 1834 cm^{-1} represents C-O stretching vibrations of α-Fe_2O_3 from Fig. 4(e) [35].

Cyclic voltammetry studies

Cyclic voltammetry (CV) analysis was carried out using potentiostat (K-Lyte 1.0) before and after dye degradation as shown in Fig. 5. The potentiostat is a three electrode assembly consisting of fabricated electrodes (N,S-TiO_2/Fe_2O_3 @Ti) as working electrode, Ag/AgCl as a reference electrode and Platinum mesh as counter electrode with 1M Na_2SO_4 as supporting electrolyte. All potentials were reported w.r.t Ag/AgCl reference electrode. The crystal violet dye concentration of 55mg/L was chosen for all voltammetric experiments and controlled current density of 0.1 mA/cm^2 was used. Cyclic voltammograms exhibit oxidation peak during forward scan and reduction peak during the reverse scan of electrolysis process. The decrease in anodic and cathodic peak currents were observed along with the time of electrolysis which indicates the oxidation of reactive azo groups [36]. The high peak current in initial CV indicates the presence of more number of reactive groups in dye molecules that leads to the higher oxidation of groups. The decrease in peak current after complete degradation indicates the reduction of reactive groups. Chrono-amperometric studies was performed at a fixed voltage (i.e. voltage where oxidation peak rises in CV) 1.2Vvs Ag/AgCl for Ti/N, S-TiO_2/Fe_2O_3 at a scan rate of 0.05V/s.

UV- Visible spectra analysis

UV-Vis analysis was used to study the electrochemical degradation of crystal violet dye using UV-Vis spectrophotometer. The intense peak of crystal violet dye absorption band was observed at λ_{max} = 576 nm and decreases with the enhancement of electrochemical treatment time. The absorption becomes zero at λ_{max}= 576nm indicates the reduction of auxochrome groups−N (CH_3) responsible for the color of crystal violet dye.

The degradation rate varies with varying of electrode assemblies. It is due to the change in an electrochemical active surface area which is responsible for adsorption of more dye molecules that interact with oxidizing agents easily. Complete decolourization can be achieved by performing electrolysis using Ti/TiO_2 and Ti/N, S-TiO_2/Fe_2O_3 electrodes in 12 h and 9 h obtained from

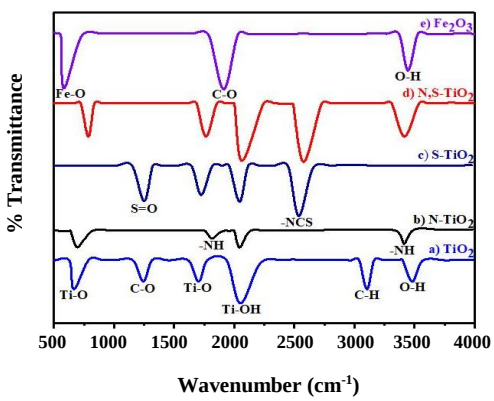

Fig. 4: FT-IR images of (a) TiO_2 (b) N- TiO_2 c) S- TiO_2 d) N, S- TiO_2 (e) Fe_2O_3 nanoparticles.

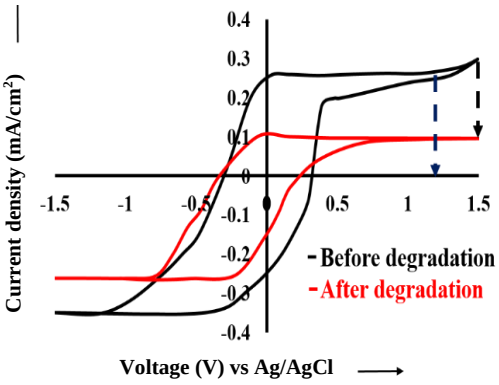

Fig. 5: Cyclic voltammetry studies of dye degradation at Ti/N,S-TiO_2/Fe_2O_3(solid line - voltage where peak rises, dotted line – decrease in peak current).

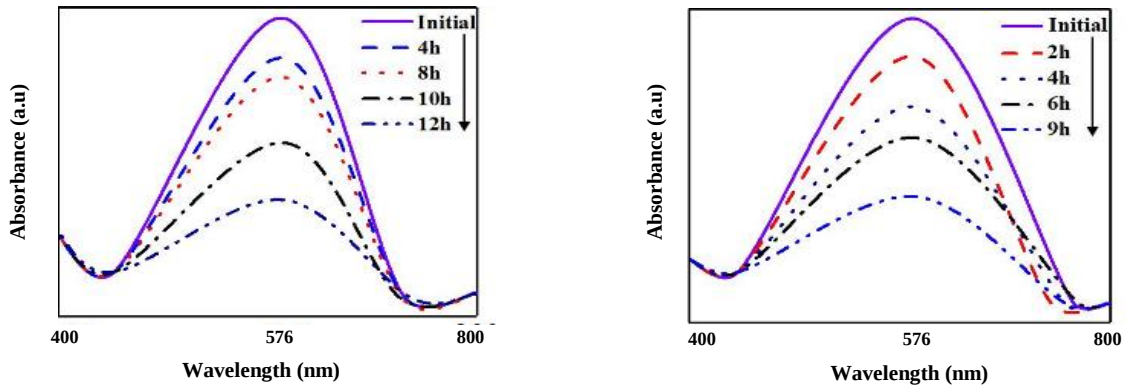

Fig. 6: Absorbance vs wavelength for a) TiO_2 b) N, S-TiO_2/Fe_2O_3 @ Ti substrate.

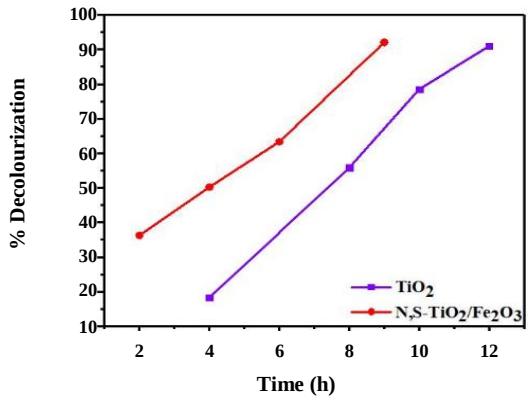

Fig. 7: Decolourization (%) vs Time (h) for TiO_2, and N, S-TiO_2/Fe_2O_3 @ Ti substrate.

UV-Vis spectra shown in Fig. 6. Hence it is concluded that N,S-TiO_2/Fe_2O_3 achieved faster degradation compared to the individual electrodes due to the interface of semiconductor material having suitable band edge positions and form Type-I heterojunction that favors charge carrier flow path. Therefore the doped metal oxide Heterostructure assemblies confirm the importance of charge carriers to achieve faster degradation and thereby enhancing degradation efficiency. Further, the decolourization efficiency at different time intervals can be calculated using formula

$$\% \text{ decolourization} = (A_0 - A) / A_0 \times 100 \quad (2)$$

Where A_0 and A are the absorbance (at the maximum wavelength, λ_{max}) of dye solution before/initial (at t = 0) and after electrochemical treatment (at t >0). The decolourization percentage (%) of crystal violet dye using Ti/TiO_2 and N, S-TiO_2/Fe_2O_3 was achieved about 91% and 92% in 12 h and 9h as shown in Fig. 7.

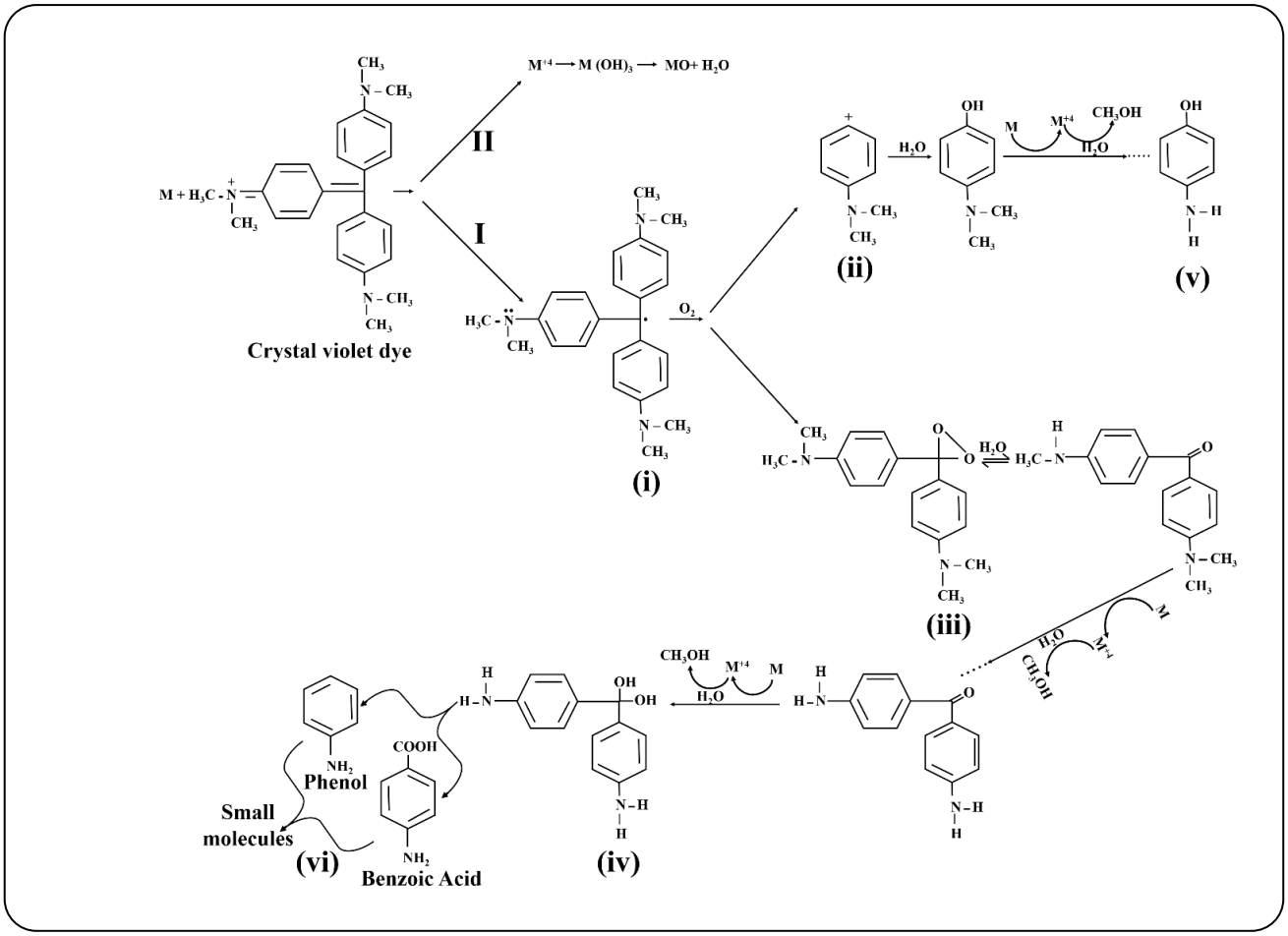

Fig. 8: Mechanism of Dye Degradation.

Mechanism of crystal violet dye degradation

Based on the literature studies an initial degradation pathway of crystal violet dye was proposed. The degradation occurs through N- dealkylation process forming a radical on central nitrogen and the destruction of chromophore structure by forming a radical on central carbon [37]. During the electrochemical treatment, the following reactions take place.

$$M \rightarrow M^{+n} + ne^- \quad (3)$$

$$2\,H_2O \rightarrow O_2 + 4H^+ + 4e^- \quad (4)$$

$$O_2 + 2H^+ + 4e^- \rightarrow H_2O_2 \quad (5)$$

$$M^{+n} + H_2O_2 \rightarrow OH^{\bullet} + OH^- \quad (6)$$

The electrons generated at the anode surface through oxidation reaction (Eq. (3)) attacks the dye molecule to destruct the conjugated structure by forming the radical on centered carbon (Fig. 8(i)) as shown in the pathway (I). The oxygen which was generated at the anode (Eq. (4)) reacts with the intermediate formed in pathway I and leads to the formation of two intermediates as shown in Fig. 8(ii) and 8(iii) and pathway II leads to formation of water molecule. Eventually, few oxygen molecules also react with electrons at the cathode surface to form hydrogen peroxide (H_2O_2) as shown in Eq. 5 which in turn used to generate $OH^{\bullet}$ radicals at the anode surface (Eq. (6)). Further N-demethylation occurs by interacting the methyl group of dye molecule with water molecule to form N-demethylated intermediate and methanol which continues till the formation of intermediates as shown in path way of Fig. 8(iv) and 8(v). Finally, phenol and benzoic acids were formed which in turn reduced to small molecules as shown in Fig. 8(vi). The $OH^{\bullet}$ radicals generated through indirect reaction (Eq. 6) acts as a strong oxidizing species for degradation of the dye molecules.

CONCLUSIONS

The present study describes the importance of doped metal oxide Heterostructure assemblies (N-S TiO_2/Fe_2O_3) in electrochemical degradation of crystal violet dye. The synthesized/fabricated electrode assemblies/nanoparticles were confirmed using different characterization techniques such as XRD, SEM, EDS, and FT-IR. Electrochemical measurements show that Ti/N, S-TiO_2/Fe_2O_3 heterostructured electrode shows better performance in comparison to the individual electrodes. This can be ascribed may be due to 1) increase in electrochemical active surface area (which accommodate more oxidants to interact with dye molecules), 2) increase in electronic conductivity due to proper band edge alignments or 3) both. The results of the current study will help to design low cost catalytic assemblies in degrading complex dyes of industrial importance.

Acknowledgments

The authors wish to thank Department of Chemical Engineering, JNTUA College of Engineering Anantapur for providing powder X-ray diffractometer facilities for XRD analysis of our samples. Authors, convey special thanks to D. Hima Bindu, for assisting in taking SEM images of our samples at IIT BHU. Further, authors wish to acknowledge OTRI-JNTUA and RIPER for providing UV-Vis and FT-IR characterizations of our sample analysis.

Received : Jun. 5, 2018 ; Accepted : Dec. 3, 2018

REFERENCES

[1] Xia Y., Dai Q., Chen J., Electrochemical Degradation of Aspirin Using a Ni Doped PbO_2 Electrode, *J. Electroanal. Chem.*, **744**: 117-125 (2015).

[2] Vignesh A., Siddarth A.S., Gokul O.S., Babu B.R., A Novel Approach for Textile Dye Degradation by Zinc, Iron–doped Tin Oxide/Titanium Moving Anode, *Int. J. Environ. Sci. Technol.*, **11**(6): 1669-1678 (2014).

[3] Li H., Zhu X., Jiang Y., Ni J., Comparative Electrochemical Degradation of Phthalic Acid Esters Using Boron-Doped Diamond and Pt Anode, *Chemosphere*, **80**(8): 845-851 (2010).

[4] Martínez-Huitle C.A., Brillas E., Decontamination of Wastewaters Containing Synthetic Organic Dyes by Electrochemical Methods: a General Review, *Appl. Catal., B*, **87**(3): 105-145 (2009).

[5] Marselli B., Garcia-Gomez J., Michaud P.A., Rodrigo M.A., Comninellis C., Electrogeneration of Hydroxyl Radicals on Boron-doped Diamond Electrodes, *J. Electrochem. Soc.*, **150**(3): D79-D83 (2003).

[6] Hammami S., Bellakhal N., Oturan N., Oturan M.A., Dachraoui M., Degradation of Acid Orange 7 by Electrochemically Generated •OH Radicals in Acidic Aqueous Medium Using a Boron-Doped Diamond or Platinum Anode: A Mechanistic Study, *Chemosphere*, **73**(5): 678-684 (2008).

[7] Migliorini F.L., Steter J.R., Rocha R.S., Lanza M.R.V., Baldan M.R., Ferreira N.G., Efficiency Study and Mechanistic Aspects in the Brilliant Green Dye Degradation Using BDD/Ti Electrodes, *Diamond Relat. Mater.*, **65**: 5-12 (2016).

[8] Hamza M., Abdelhedi R., Brillas E., Sirés I., Comparative Electrochemical Degradation of the Triphenylmethane Dye Methyl Violet with Boron-Doped Diamond and Pt Anodes, *J. Electroanal. Chem.*, **627**(1): 41-50 (2009).

[9] Chianca de Moura D., Quiroz M.A., Ribeiro da Silva D., Salazar R., Martínez-Huitlea C.A., Electrochemical Degradation of Acid Blue 113 Dye Using TiO_2-Nanotubes Decorated with PbO_2 as Anode, *Environ. Nanotechnol. Monit. Manag.*, **5**: 13-20(2016).

[10] Sopaj F., Rodrigo M.A., Oturan N., Podvorica F.I., Pinson J., Oturan M.A., Influence of the Anode Materials on the Electrochemical Oxidation Efficiency. Application to Oxidative Degradation of the Pharmaceutical Amoxicillin, *Chem. Eng. J.*, **262**: 286-294 (2015).

[11] Panizza M., Importance of Electrode Material in the Electrochemical Treatment of Wastewater Containing Organic Pollutants, in "Electrochemistry for the Environment", Springer, New York (2010).

[12] Xu L., Liang G., YinM., A Promising Electrode Material Modified by Nb-doped TiO_2 Nanotubes for Electrochemical Degradation of AR 73, *Chemosphere*, **173**: 425-434 (2017).

[13] Hu X., Li G., Yu J.C., Design, Fabrication, and Modification of Nanostructured Semiconductor Materials for Environmental and Energy Applications, *Langmuir*, **26**(5): 3031-3039 (2009).

[14] Lingampalli S.R., Ayyub M.M., Rao C.N. ., Recent Progress in the Photocatalytic Reduction of Carbon Dioxide, *ACS Omega*, **2**(6): 2740-2748(2017).

[15] Zhan W.W., Kuang Q., Zhou J.Z., Kong X.J., Xie Z.X., Zheng L.S., Semiconductor@ Metal–Organic Framework Core–Shell Heterostructures: A Case of Zno@ ZIF-8 Nanorods with Selective Photoelectrochemical Response, *J. Am. Chem. Soc.*, **135**(5): 1926-1933 (2013).

[16] Behara D.K., Sharma G.P., Upadhyay A.P., Gyanprakash M., Pala R.G.S., Sivakumar S., Synchronization of Charge Carrier Separation by Tailoring the Interface of Si–Au–TiO_2 Heterostructures *via* Click Chemistry For PEC Water Splitting, *Chem. Eng. Sci.*, **154**: 150-169 (2016).

[17] Chan S.H.S., Yeong Wu T., Juan J.C., Teh, C.Y., Recent Developments of Metal Oxide Semiconductors as Photocatalysts In Advanced Oxidation Processes (Aops) For Treatment Of Dye Wastewater, *J. Chem. Technol. Biotechnol.*, **86**(9): P.1130-1158 (2011).

[18] Kumar S.G., Devi L.G., Review on Modified TiO_2 Photocatalysis Under UV/Visible Light: Selected Results And Related Mechanisms on Interfacial Charge Carrier Transfer Dynamics, *J. Phys. Chem. A*, **115**(46): 13211-13241 (2011).

[19] Zatloukalová K., Obalová L., Koči K., Čapek L., Matěj Z., Šnajdhaufová H., Ryczkowski J., Słowik G., Photocatalytic Degradation of Endocrine Disruptor Compounds in Water Over Immobilized TiO_2 Photocatalysts, *Iran. J. Chem. Chem. Eng. (IJCCE)*, **36**(2): 29-38 (2017).

[20] He L., Jing L., Luan Y., Wang L., Fu H., Enhanced Visible Activities of A-Fe_2O_3 by Coupling N-Doped Graphene and Mechanism Insight, *ACS Catal.*, **4**(3): 990-998 (2014).

[21] Ramacharyulu P.V.R.K., Nimbalkar D.B., Kumar J.P., Prasad G.K., Ke, S.C., N-Doped, S-Doped TiO_2 Nanocatalysts: Synthesis, Characterization and Photocatalytic Activity in the Presence of Sunlight, *RSC Adv.*, **5**(47): 37096-37101 (2015).

[22] Diwald O., Thompson T.L., Zubkov T., Goralski E.G., Walck S.D., Yates J.T., Photochemical Activity of Nitrogen-Doped Rutile TiO_2 (110) in Visible Light, *J. Phys. Chem. B*, **108**(19): 6004-6008 (2004).

[23] Gholipour M.R., Dinh C.T., Béland F., Do T.O., Nanocomposite Heterojunctions as Sunlight-Driven Photocatalysts for Hydrogen Production from Water Splitting, *Nanoscale*, **7**(18): 8187-8208 (2015).

[24] Liu G., Wang L., Yang H.G., Cheng H.M., Lu G.Q.M., Titania-Based Photocatalysts-Crystal Growth, Doping and Heterostructuring, *J. Mater. Chem.*, **20**(5): 831-843 (2010).

[25] Duan T., Chen Y., Wen Q., Duan Y., Different Mechanisms and Electrocatalytic Activities of Ce Ion or Ceo_2 Modified Ti/Sb–Sno_2 Electrodes Fabricated by One-Step Pulse Electro-Codeposition, *RSC Adv.*, **5**(25): 19601-19612 (2015).

[26] Rao A.N.S., Venkatarangaiah V.T., Metal Oxide-Coated Anodes in Wastewater Treatment, *Environ. Sci. Pollut. Res.*, **21**(5): 3197-3217 (2014).

[27] Xu Y., Schoonen M.A., The Absolute Energy Positions of Conduction and Valence Bands of Selected Semiconducting Minerals, *Am. Mineral.*, **85**(3-4): 543-556 (2000).

[28] Behara D.K., Ummireddi A.K., Aragonda V., Gupta P.K., Pala R.G.S., Sivakumar S., Coupled Optical Absorption, Charge Carrier Separation, and Surface Electrochemistry in Surface Disordered/Hydrogenated TiO_2 for Enhanced PEC Water Splitting Reaction, *Phys. Chem. Chem. Phys.*, **18**(12): 8364-8377 (2016).

[29] Bagheri S., Chandrappa K., Hamid S.B.A., Generation of Hematite Nanoparticles *via* Sol-Gel Method, *Res. J. Chem. Sci.*, **3**(7): 62-68 (2013).

[30] Grandcolas M., Ye J., Preparation of Fine, Uniform Nitrogen-and Sulfur-Modified TiO_2 Nanoparticles from Titania Nanotubes, *Sci. Technol. Adv. Mater.*, **11**(5): 055001 (2010).

[31] Wang C., Hu Q., Huang J., Wu L., Deng Z., Liu Z., Liu Y., Cao Y., Efficient Hydrogen Production by Photocatalytic Water Splitting Using N-Doped TiO_2 Film, *Appl. Surf. Sci.*, **283**: 188-192 (2013).

[32] Liu Q., Cao F., Wu F., Tian, W., Li L., Interface Reacted $Znfe_2o_4$ on A-Fe_2O_3nanoarrays for Largely Improved Photo Electrochemical Activity, *RSC Adv.*, **5**(97): 79440-79446 (2015).

[33] Randeniya L.K., Murphy A.B., Plumb I.C., A Study of S-Doped TiO_2 for Photoelectrochemical Hydrogen Generation from Water, *J. Mater. Sci.*, **43**(4): 1389-1399 (2008).

[34] Ivanov S., Barylyak A., Besaha K., Bund A., Bobitski Y., Wojnarowska-Nowak R., Yaremchuk I., Kus-Liśkiewicz M., Synthesis, Characterization, and Photocatalytic Properties of Sulfur-and Carbon-Codoped TiO_2 Nanoparticles, *Nanoscale Res. Lett.*, **11**(1): 140 (2016).

[35] Satheesh R., Vignesh K., Suganthi A., Rajarajan M., Visible Light Responsive Photocatalytic Applications of Transition Metal (M= Cu, Ni and Co) Doped A-Fe_2O_3 Nanoparticles, *J. Environ. Chem. Eng.*, **2**(4): 1956-1968 (2014).

[36] Khan M.M., Lee J., Cho M.H., Au@ TiO_2 Nanocomposites for the Catalytic Degradation of Methyl Orange and Methylene Blue: an Electron Relay Effect, *J. Ind. Eng. Chem.*, **20**(4): 1584-1590 (2014).

[37] Singh S., Srivastavav C., Malld., Mechanism of Dye Degradation During Electrochemical Treatment, *J. Phys. Chem. C*,**117**(29): 15229-15240 (2013).